Available online at www.sciencedirect.com
SCIENCE DIRECT®
Journal of Magnetism and Magnetic Materials ▮ (▮▮▮▮) ▮▮▮–▮▮▮
Journal of magnetism and magnetic materials
www.elsevier.com/locate/jmmm

The influence of composition and field annealing on magnetic properties of FeCo-based amorphous and nanocrystalline alloys

F. Johnson[a,*], C.Y. Um[b], M.E. McHenry[b], H. Garmestani[c]

[a]*National Institute of Standards and Technology, Stop 8552, 100 Bureau Drive, Gaithersburg, MD 20899, USA*
[b]*Carnegie Mellon University, USA*
[c]*Georgia Institute of Technology, USA*

Received 14 December 2004; received in revised form 20 January 2005

Abstract

We report the influence of composition and very high transverse field annealing on the magnetic properties and structure of four FeCo-based amorphous and nanocrystalline alloys. The compositions $(Fe_{50}Co_{50})_{89}Zr_7B_4$ and $(Fe_{65}Co_{35})_{89}Zr_7B_4$ were investigated changing the Fe:Co ratio from 50:50 to 65:35. $(Fe_{50}Co_{50})_{85}Zr_2Nb_4B_{8.5}$ was chosen to investigate Nb substitution for Zr in an FeCo-based alloy. This substitution is shown to increase the magnetostrictive constant, λ_S, of the nanocrystalline alloy from 36×10^{-6} to 54×10^{-6}. The composition $(Fe_{65}Co_{35})_{84}Cr_5Zr_7B_4$ was studied to investigate the influence of Cr on intergranular coupling across the amorphous matrix. Samples of each composition were annealed in the amorphous state at 300 °C and in the nanocrystalline state at 600 °C. Field annealing was performed in 17 T transverse field in an inert atmosphere. Frequency-dependent magnetic properties were measured with an automatic recording hysteresisgraph. Static magnetic properties were measured with a vibrating sample magnetometer. The mass-specific power loss of the alloys decreased with field annealing in both the nanocrystalline and amorphous states for some frequency and induction combinations. Furthermore, the hysteresis loops are sheared after field annealing, indicating a transverse magnetic anisotropy. The nanocrystalline $(Fe_{50}Co_{50})_{85}Zr_2Nb_4B_{8.5}$ composition has a lower relative permeability than the other compositions.
Published by Elsevier B.V.

PACS: 75.75.+a; 75.50.Kj; 75.50.Bb; 81.40.Rs

Keywords: Nanocrystalline alloys; Amorphous alloys; Field annealing; Power loss; Soft magnets

*Corresponding author. Tel.: +301 975 4936; fax: +301 975 4552.
E-mail address: frank.johnson@nist.gov (F. Johnson).

0304-8853/$ - see front matter Published by Elsevier B.V.
doi:10.1016/j.jmmm.2005.02.056

1. Introduction

Nanocrystalline soft magnetic alloys are comprised of nanocrystalline grains embedded in an amorphous matrix. Alloys based on the FeCo system were first reported by Müller et al. [1] and their high-temperature properties were explored by Willard et al. [2], who named them HITPERM. Willard et al. also demonstrated that HITPERM contains ordered α'-FeCo grains and has an amorphous matrix enriched in Co. The amorphous Curie temperature (T_c) of HITPERM is higher than other, non-Co-containing nanocrystalline alloys. HITPERM's high amorphous T_c enables its nanocrystalline grains to remain exchange coupled at high temperatures [3]. Recent work has focused on modifying the original HITPERM alloy ($Fe_{44}Co_{44}Zr_7B_4Cu_1$) with the goal of reducing the hysteretic power loss while maintaining high-temperature operability [4]. Other goals have included studies of crystallization kinetics as well as the partitioning of Fe and Co between the crystalline and amorphous phases [5]. Recent availability of very high magnetic field annealing furnaces has opened a new research avenue for nanocrystalline alloys. Previously, the effects of field annealing on the original HITPERM's magnetic properties have been reported [6].

The goal of this work was to identify routes by which the magnetic properties, particularly the hysteretic power loss, may be improved. Likely compositional variations, as well as very high field annealing, were systematically investigated. Four derivatives of HITPERM were selected. $Fe_{44.5}Co_{44.5}Zr_7B_4$ (50:50) is closest to the originally reported HITPERM alloy and was studied to verify previously reported results. $Fe_{57.85}Co_{31.15}Zr_7B_4$ (65:35) changes the Fe:Co ratio from 50:50 to 65:35, increasing the saturation magnetization (M_S) and the first anisotropy constant of the bulk alloy, and is expected to also change the nanocrystalline alloy's properties. $Fe_{42.75}Co_{42.75}Zr_2Nb_4B_{8.5}$ (Nb-containing) was chosen to study the influence of substituting Nb for Zr on the magnetic properties, inspired by Makino et al.'s [7] success in finding a near-zero magnetostrictive Nb-containing NANOPERM. $Fe_{54.6}Co_{29.4}Cr_5Zr_7B_4$ (Cr-containing) was studied to investigate the influence of Cr on intergranular coupling.

Very high field annealing was used to induce a transverse magnetic anisotropy in the samples. The field was oriented transverse to the circumference of the wound, toroidal-shaped samples, in the plane of the ribbon. Such a transverse anisotropy will promote rotational, reversible magnetization processes, reducing hysteretic power loss. Diffusional pair-ordering of unlike atoms is considered as a possible source of field-induced anisotropy [8], if other sources of anisotropy such as preferred orientation of the grains can be disregarded. The samples were annealed in both the nanocrystalline and amorphous states.

2. Procedure

Prealloyed ingots were rapidly solidified by melt spinning into amorphous ribbons 2–5 mm wide, 25–50 μm thick, and several meters long. The ribbons were wound onto toroidal bobbin cores for AC magnetic properties measurements. Sample volume was calculated by multiplying the width, thickness and length of the wound ribbon. Cross-sectional area of the cores was calculated by multiplying the thickness and width of the ribbons with the number of wraps around the bobbin. Samples for static magnetic measurements and structural analysis were mounted flat between pyrex slides to avoid the acquisition of curvature during annealing.

Annealing was performed in a resistive tube furnace under Ar. Very high field annealing was performed in a resistive solenoidal magnet at the National High Field Magnet Laboratory in Tallahassee, FL. The amorphous (am) sample was first annealed in zero field for 3600 s, measured, then field annealed at 17 T for 3600 s and then measured. The nanocrystalline (nc) sample was first annealed at zero field for 3600 s to form the nanocrystalline state, then measured. The nc sample was then field annealed at 17 T for 3600 s and measured again.

The annealing temperatures were chosen to maintain the amorphous state or achieve the nanocrystalline state of the samples. A temperature of 600 °C is sufficient to drive the nanocrystallization reaction to completion within an hour [9].

Further structural evolution at 600 °C is minimal within a time scale of several hours. A temperature of 300 °C is not sufficient to start crystallization on the time scale of several hours but is sufficient to relax any residual stress from the rapid solidification process [10]. Thus the samples annealed at 300 °C will remain in the amorphous condition.

Saturation magnetization (M_S) and static coercivity (H_C) were measured with an ADE 10 vibrating sample magnetometer [11] (VSM). The applied field was aligned parallel to the plane of the ribbon to minimize demagnetizing fields. AC magnetic properties were measured with a Walker AMH-401A hysteresisgraph. X-ray diffraction was performed with a Phillips X'Pert diffractometer both in conventional and in-plane sample geometries (Fig. 1). Saturation magnetostriction of some samples were measured via a strain gage technique.

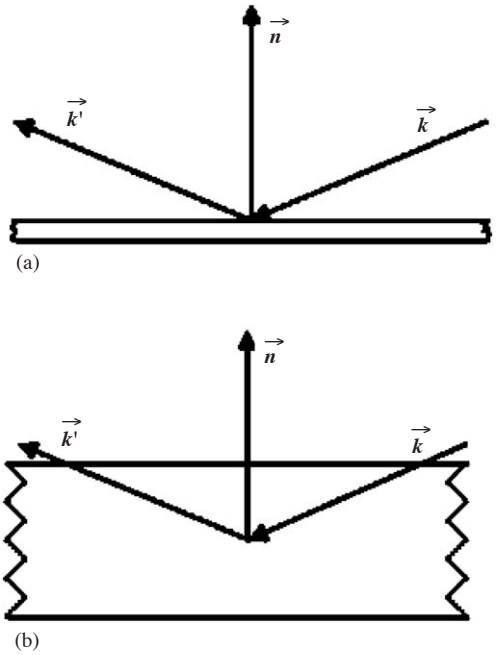

Fig. 1. Illustration of geometries for (a) conventional and (b) in-plane X-ray diffraction. $\vec{k}$ is the incident X-ray beam, $\vec{k}'$ is the diffracted X-ray beam, and $\vec{n}$ is the vector normal to the diffracting planes that satisfy Bragg's law. In the conventional geometry the diffracted plane normals are perpendicular to the surface of the ribbon, whereas in the in-plane geometry the diffracted plane normals are nearly parallel to the surface of the ribbon.

3. Results

3.1. Static magnetic measurements

Table 1 presents the M_S and H_C of the samples in the nanocrystalline (nc) and amorphous (am) states. Field annealing does not have an effect on M_S or static H_C. The trend of H_C with annealing temperature and composition is less distinct than M_S. This is due to the 8 A/m field resolution of the VSM used to make these measurements. The magnetostrictive coefficient (λ_S) of the nanocrystalline Nb-containing alloy was measured to be 54×10^{-6}. This compared to a previously reported value of 36×10^{-6} for the nanocrystalline 50:50 alloy [6].

Table 1
Saturation magnetization (M_S) and coercivity (H_C) measured by VSM in the nanocrystalline (nc) and amorphous (am) states

Comp.	M_s (A m^2/kg)		H_c (A/m)	
	nc	am	nc	am
50:50	173	158	16	56
65:35	180	169	<8	16
Zr:Nb	175	158	220	16
Cr-sub.	149	131	100	<8

3.2. Frequency-dependent magnetic properties

Fig. 2 presents the hysteresis loop for nanocrystalline 50:50 alloy measured at a frequency of 1 kHz to an induction of 0.5 T. The loop was measured on the same sample before (Step 1) and after (Step 2) field annealing. Field annealing caused a shear of the hysteresis loop. For all alloys except amorphous Cr-containing ones, the hysteresis loops measured in the nanocrystalline state are sheared relative to the hysteresis loops measured in the amorphous state. The nanocrystalline Nb-containing alloy has a hysteresis loop

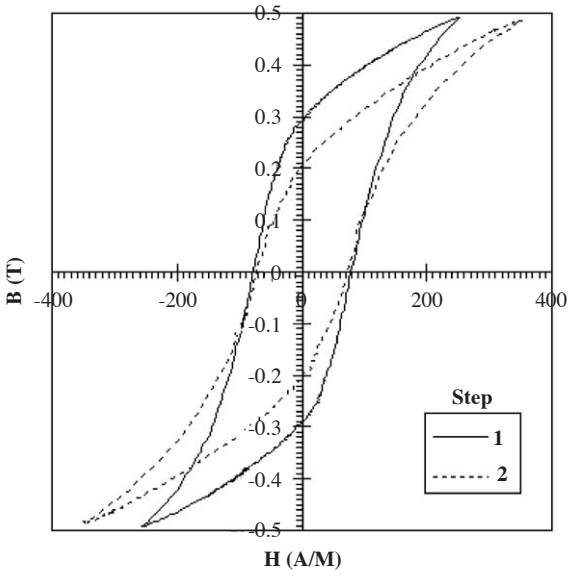

Fig. 2. Hysteresis loop for nanocrystalline 50:50 alloy, measured at 1 kHz at 0.5 T B_{MAX}. Solid curve, labeled 1, measured before field annealing (Step 1). Dashed curve, labeled 2, measured after field annealing (Step 2).

sheared to a greater relative extent than the other alloys.

Tables 2 and 3 present the permeability (μ) and power loss of the nanocrystalline and amorphous samples in the before and after field annealed condition. The nanocrystalline samples generally have lower μ but higher power loss than the amorphous samples. The nanocrystalline Nb-containing alloy is observed to have a lower μ compared to other nanocrystalline alloys. Field annealing is generally observed to lower the μ and power loss of both the nanocrystalline and amorphous alloys. A notable exception is that field annealing the amorphous Cr-containing alloy is observed to increase μ.

3.3. X-ray diffraction

Fig. 3 presents the conventional and Fig. 4 presents the in-plane X-ray diffraction pattern of the nanocrystalline 50:50 alloy in the before field annealing (Step 1) and after field annealing (Step 2). No shift in ratios of peak intensities in either geometry due to field annealing was observed in any of the alloys. This suggests that in-plane crystalline texture was not influenced by field annealing.

Table 2
Relative permeability $[(\mu/\mu_o)\times 10^{-3}]$, calculated as B_{MAX}/H_{MAX}, measured at 1 kHz and 0.5 T B_{MAX}, for nanocrystalline (nc) and amorphous (am) alloys, before field annealing (Step 1) and after field annealing (Step 2)

Comp.	nc		am	
	Step 1	Step 2	Step 1	Step 2
50:50	1555	1120	2067	801
65:35	3651	2296	2572	1300
Zr:Nb	675	464	1918	1483
Cr-sub.	2792	1650	1634	3265

Table 3
Power loss, in W/kg measured at 1 kHz and 0.5 T B_{MAX}, for nanocrystalline (nc) and amorphous (am) alloys, before field annealing (Step 1) and after field annealing (Step 2)

Comp.	nc		am	
	Step 1	Step 2	Step 1	Step 2
50:50	24.2	20.1	7.20	14.1
65:35	17.5	16.9	21.2	19.4
Zr:Nb	39.4	38.3	26.4	28.7
Cr-sub.	27.3	16.7	18.4	11.8

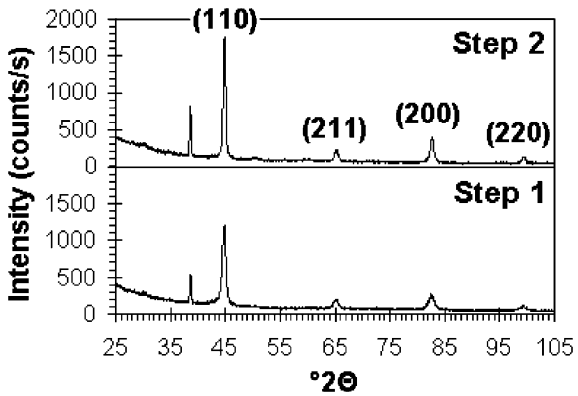

Fig. 3. X-ray diffraction patterns of nanocrystalline 50:50 alloy measured before (Step 1) and after (Step 2) field annealing at 600 °C. Incident X-ray beam was oriented perpendicularly to ribbon surface. Plane indices in parentheses. Unidentified low angle peak is oxide.

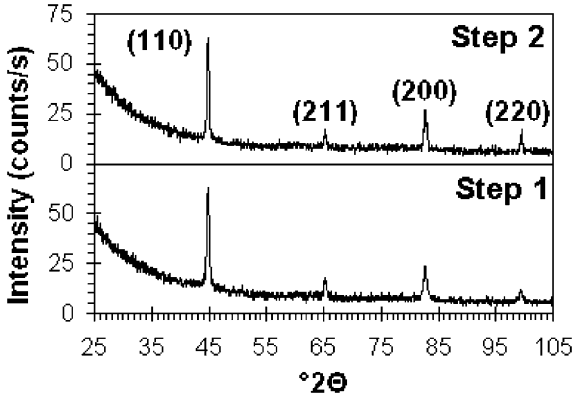

Fig. 4. In-plane X-ray diffraction patterns of nanocrystalline 50:50 alloy measured before (Step 1) and after (Step 2) field annealing at 600 °C. Incident X-ray beam was oriented nearly parallel to ribbon surface. Plane indices in parentheses.

4. Discussion

4.1. Influence of field annealing

Field annealing is observed to be more effective in reducing power loss in nanocrystalline alloys than in amorphous alloys. The μ is reduced in both the nanocrystalline and amorphous phases by field annealing. Here, μ is calculated as B_{MAX}/H_{MAX}, and is neither initial μ nor maximum differential μ. This definition of μ is frequently used when evaluating magnetic devices which are required to exhibit linear response, as it would be a likely application for the presently studied materials. The change in μ was observed on the same sample in the before and after field annealed state, and care was taken to consistently prepare the samples for the AC measurement. Thus it is reasonable to conclude that the change in μ is caused by the field annealing process. The source for the larger effect on power loss in the nanocrystalline state is the higher annealing temperature than that used in the amorphous state (600 °C vs. 300 °C). One cause of the formation of a field-induced anisotropy is a diffusional process involving the production of ordered atomic pairs. Annealing at a higher temperature causes larger atomic mobility, enabling faster diffusion. The annealing temperature of the amorphous phase is limited by the primary crystallization temperature, which is ~500 °C for HITPERM [12]. A temperature of 300 °C was chosen to allow stress relief while avoiding crystallization. Annealing the amorphous samples at temperatures higher than 300 °C but lower than the crystallization temperature may induce a larger anisotropy.

High-temperature field annealing presented the possibility that the crystallographic texture of the nanocrystalline grains might be modified. Subtle changes in structure have been detected in nanocrystalline alloys annealed in a stress field [13]. In a magnetic field grains may grow along the magnetically "soft" {1 0 0} axes of α'-FeCo, resulting in a preferred orientation of (1 0 0) planes transverse to the ribbon length. In-plane X-ray diffraction would display a shift in peak intensity ratios favoring (1 0 0). This was not observed in any alloy, suggesting that field induced anisotropy was not due to a measurable, in-plane crystalline texture.

4.2. Influence of composition

The M_S of the 65:35 alloy increased with respect to the 50:50 alloy in both the amorphous and nanocrystalline states. The crystalline Nb-containing alloy had an M_S comparable to the 65:35 alloy, but the higher concentration of B in the Nb-containing alloy yields a lower density and thus a lower M_S per unit volume. The Cr-containing alloy had substantially reduced M_S in both the nanocrystalline and amorphous phases. Cr is known to reduce ferromagnetic intergranular coupling when used as an alloy addition in recording media [14].

The Nb-containing alloy is notable in that the μ of the nanocrystalline phase is lower than the other alloys, and the H_C is higher. This may be partially explained by a large magnetostrictive constant in the Nb-containing alloy leading to a large magnetoelastic anisotropy. The H_C of the nanocrystalline Cr-containing alloy was higher than the nanocrystalline 50:50 or 65:35 alloys, due to reduced intergranular coupling.

5. Conclusions

Field annealing is shown to reduce the power loss more effectively in the nanocrystalline HITPERM

alloys than in the amorphous state. The μ and power loss can be reduced for some HITPERM alloys by field annealing. The crystalline texture of the nanocrystalline grains was not observed to be affected by field annealing, suggesting that a diffusional process such as pair ordering is the source of the induced anisotropy. Adjusting the ratio of Fe:Co in HITPERM from 50:50 to 65:35 increases the M_S and μ. A substantial change in μ and H_C is observed in HITPERM where the glass-forming element Nb is substituted for Zr. This is partially explained by an increase in the λ_S of the Nb-containing alloy. Substituting Cr for Fe and Co in HITPERM substantially reduces the M_S of the amorphous and crystalline alloys and increases the H_C of the nanocrystalline alloy relative to the other alloys.

Acknowledgments

This work was supported in part by a NASA Graduate Student Researcher Fellowship (Grant no. NGT3-52379), an Air Force Dual Use Science & Technology (Air Force Research Lab ♯ F33615-02-2241) contract administered by the Wright Patterson AFB, and Magnetics Inc., a division of Spang, Inc.

References

[1] M. Müller, H. Grahl, N. Mattern, U. Kuhn, B. Schnell, J. Magn. Magn. Mater. 160 (1996) 284.

[2] M.A. Willard, D.E. Laughlin, M.E. McHenry, D. Thoma, K. Sickafus, J.O. Cross, V.G. Harris, J. Appl. Phys. 84 (1998) 6772.

[3] F. Johnson, A. Hsiao, C. Ashe, D.E. Laughlin, D. Lambeth, M.E. McHenry, L.K. Varga, First IEEE Conference on Nanotechnology, Maui, 2001, pp. 1–6.

[4] M.A. Willard, J.C. Claassen, R.M. Stroud, T.L. Francavilla, V.G. Harris, IEEE Trans. Magn. 38 (2002) 3045.

[5] Y. Zhang, J.S. Blazquez, A. Conde, P.J. Warren, A. Cerezo, Mater. Sci. Eng. A 353 (2003) 158.

[6] F. Johnson, H. Garmestani, S.Y. Chu, M.E. McHenry, D.E. Laughlin, IEEE Trans. Magn. 40 (2004) 4.

[7] A. Makino, T. Bitoh, A. Kojima, A. Inoue, T. Masumoto, J. Magn. Magn. Mater. 215 (2000) 288.

[8] S. Chikazumi, Physics of Ferromagnetism, second ed., Oxford University Press, New York, 1997, pp. 299–309.

[9] A. Hsiao, M.E. McHenry, D.E. Laughlin, M.J. Kramer, C. Ashe, T. Ohkubo, IEEE Trans. Magn. 38 (2002) 3039.

[10] F.E. Luborsky, J.L. Walter, IEEE Trans. Magn. 13 (1977) 1635.

[11] Certain commercial equipment, instruments, or materials are identified in this paper to specify the experimental procedure adequately. Such identification is not intended to imply recommendation or endorsement by the National Institute of Standards and Technology, nor is it intended to imply that the materials or equipment identified are necessarily the best available for the purpose.

[12] F. Johnson, R. Hughes, R. Gallagher, D.E. Laughlin, M.E. McHenry, M.A. Willard, V.G. Harris, IEEE Trans. Magn. 37 (2001) 2261.

[13] M. Ohnuma, K. Hono, T. Yanai, H. Fukunaga, Y. Yoshizawa, Appl. Phys. Lett. 83 (2003) 2859.

[14] R.M. White, Introduction to Magnetic Recording, IEEE Press, New York, 1985, p. 17.